

# The physics potential of HE-LHC

## Editors:

**Workshop steering group:** A. Dainese, M.L. Mangano, A.B. Meyer, A. Nisati, G.P. Salam, M. Vesterinen

**WG1 conveners:** P. Azzi, S. Farry, P. Nason, A. Tricoli, and D. Zeppenfeld

**WG2 conveners:** M. Cepeda, S. Gori, P. J. Ilten, M. Kado, and F. Riva,

**WG3 conveners:** X. Cid-Vidal, M. D’Onofrio, P. J. Fox, R. Torre, and K. Ulmer

**WG4 conveners:** A. Cerri, V.V. Gligorov, S. Malvezzi, J. Martin Camalich, and J. Zupan

**WG5 conveners:** Z. Citron, J. F. Grosse-Oetringhaus, J. M. Jowett, Y.-J. Lee, U. Wiedemann, M. Winn

**Contributing authors:** see Addendum

## ABSTRACT

This document summarizes the physics potential of the High-Energy LHC (HE-LHC), under consideration as a possible future project at CERN. The HE-LHC is a 27 TeV pp collider, to be installed in the LHC tunnel, relying on the 16 T magnet technology being developed for the 100 TeV Future Circular Collider (FCC-hh). The HE-LHC is designed to deliver 10-15  $\text{ab}^{-1}$  of integrated luminosity to two general purpose detectors, during 20 years of operation. As for the LHC, the facility could host a dedicated interaction point focused on flavour physics, delivering 3  $\text{ab}^{-1}$  of integrated luminosity to an upgraded LHCb detector, and would continue the programme of heavy ion collisions. The results presented here were obtained in the context of the Workshop on “The physics of HL-LHC, and perspectives on HE-LHC”, which ran for over a year after its kick-off meeting on 30 October – 1 November 2017. These studies complemented those focused on the engineering and technological aspects of the project, performed in the context of the FCC conceptual design report (CDR) for the HE-LHC, and documented elsewhere [1]. The activity has been carried out by five working groups (WGs): “Standard Model” (WG1), “Higgs” (WG2), “Beyond the Standard Model” (WG3), “Flavour” (WG4) and “QCD matter at high density” (WG5). The reports from the WGs, extending this executive summary with much more detail and many more results, are available on the CERN Document Server [2–6], and will appear on arXiv. The documents describing in full detail the HL-LHC and HE-LHC studies performed by the ATLAS and CMS Collaborations can be found in Ref. [7] (available in early 2019).

## References

1. M. Benedikt, J. Gutleber, and F. Zimmermann, (editors), *Future Circular Collider Study. Volume 4: The High Energy LHC (HE-LHC) Conceptual Design Report*, CERN-ACC-2018-0059, CERN, Geneva, Dec, 2018. Submitted to Eur. Phys. J. ST. <http://cern.ch/go/S9Gq>.
2. P. Azzi, S. Farry, P. Nason, A. Tricoli, and D. Zeppenfeld, (conveners), et al, *Standard Model Physics at the HL-LHC and HE-LHC*, CERN-LPCC-2018-03, CERN, Geneva, 2018. <https://cds.cern.ch/record/2650160>.
3. M. Cepeda, S. Gori, P. J. Ilten, M. Kado, and F. Riva, (conveners), et al, *Higgs Physics at the HL-LHC and HE-LHC*, CERN-LPCC-2018-04, CERN, Geneva, 2018. <https://cds.cern.ch/record/2650162>.
4. X. Cid-Vidal, M. D’Onofrio, P. J. Fox, R. Torre, and K. Ulmer, (conveners), et al, *Beyond the Standard Model Physics at the HL-LHC and HE-LHC*, CERN-LPCC-2018-05, CERN, Geneva, 2018. <https://cds.cern.ch/record/2650173>.
5. A. Cerri, V. V. Gligorov, S. Malvezzi, J. Martin Camalich, and J. Zupan, (conveners), et al, *Flavour Physics at the HL-LHC and HE-LHC*, CERN-LPCC-2018-06, CERN, Geneva, 2018. <https://cds.cern.ch/record/2650175>.
6. Z. Citron, A. Dainese, J. F. Grosse-Oetringhaus, J. M. Jowett, Y.-J. Lee, U. Wiedemann, and M. A. Winn, (conveners), et al, *Future physics opportunities for high-density QCD at the LHC with heavy-ion and proton beams*, CERN-LPCC-2018-07, CERN, Geneva, 2018. [arXiv:1812.06772](https://arxiv.org/abs/1812.06772) [hep-ph]. <https://cds.cern.ch/record/2650176>.
7. The ATLAS and CMS Collaborations, *Report on the Physics at the HL-LHC and Perspectives for the HE-LHC*, CERN-LPCC-2019-01, CERN, Geneva, 2019. <https://cds.cern.ch/record/2651134>.

# 1 Introduction

The potential physics returns of the HE-LHC can be grouped into four areas:

1. extending the HL-LHC reach in direct searches for new particles, approximately doubling the reach in mass;
2. establishing the structure of the symmetry-breaking Higgs potential, which lies at the heart of the Standard Model's (SM) electroweak (EW) sector;
3. improving the precision of the HL-LHC measurements, in the EW and flavour sectors, with a consequently better indirect sensitivity to new physics at high mass scales, and better direct sensitivity to elusive final states such as dark matter (DM);
4. exploring in greater detail the properties of possible future LHC discoveries, confirming preliminary signs of discovery from the LHC, or identifying the underlying origin of new phenomena revealed indirectly (e.g. the flavour anomalies currently under discussion) or in experiments other than those of the LHC (e.g. DM or neutrino experiments).

The first three areas offer guaranteed deliverables, with targets that can be defined today. On the other hand, only future data will enable the qualification and quantification of the relevance of the fourth area in the planning for the HE-LHC, and a few scenarios can be considered today as examples.

The studies performed during the workshop were mostly of phenomenological nature, since there is currently no effort to design an HE-LHC detector. The experimental environment (radiation flux, track densities, event pile-up) at HE-LHC will be very similar to the FCC-hh, and the technological progress projected for a future FCC-hh detector can help define the HE-LHC detector design. However, the design is tightly constrained by the boundary conditions: the existing caverns' size, the infrastructure and the presence of the current detectors. While detailed studies of possible upgrade or replacement options for the ATLAS and CMS detectors have not been investigated, the physics studies presented here generally assume typical ATLAS and CMS HL-LHC detector performances, modelled via Delphes.

## 2 The direct discovery reach of HE-LHC

The HE-LHC is expected to extend the mass reach for the discovery of new particles by a factor of  $\sim 2$  with respect to HL-LHC. While the study of individual scenarios must account in detail for the possibly different evolution of signals and backgrounds with beam energy and include the new analysis opportunities offered by the larger statistics and kinematic reach available at 27 TeV, it is possible to provide general estimates of the improved sensitivity by extrapolating the partonic luminosities that are relevant for the production of various final states. This is shown in Fig. 1, where the extension sensitivity relative to the HL-LHC is given, for states produced via different initial states. For example, new gauge bosons such as a  $Z'$ , whose reach at the HL-LHC is estimated to be in the range of 6 TeV, could be observed by the HE-LHC up to a mass of  $\sim 12$  TeV. This qualitative conclusion has been verified by the more detailed studies carried out so far, as shown in the examples below.

In several BSM scenarios an extension in reach by a factor of two relative to the HL-LHC may be small compared to the large range of possible masses. However, in several interesting new physics scenarios, the doubling in reach allows coverage of a large fraction of the relevant parameter space. A subset of concrete examples are highlighted here, selected among a large number of studies presented in the Workshop reports. All quoted exclusion (discovery) reach values refer to 95% CL ( $5\sigma$ ).

### 2.1 Supersymmetry

The increase in energy from 14 TeV to 27 TeV leads to a large increase in the production cross section of heavy coloured states, e.g. a 3.5 TeV gluino has a nearly 400-fold increase in production cross section. For supersymmetric spectra without compression the HE-LHC has 95% CL sensitivity to gluinos ( $\tilde{g}$ ) up to masses of 6 TeV and discovery potential up to 5.5 TeV. Exclusion and discovery reaches for top squarks ( $\tilde{t}$ ) are up to 3.5 TeV and 3 TeV, respectively. These results shed some light

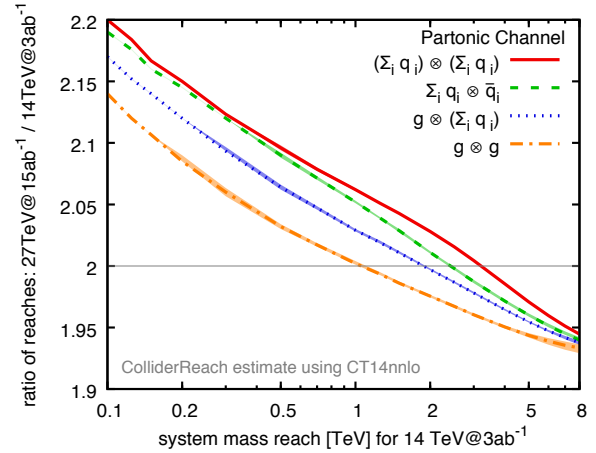


**Figure 1.** Estimate of the system mass (e.g.  $m_{Z'}$  or  $2m_{\tilde{g}}$ ) that can be probed in searches for new particles at HE-LHC, given an established reach at HL-LHC. The lines' width reflects the PDF uncertainty.

All quoted exclusion (discovery) reach values refer to 95% CL ( $5\sigma$ ).

on the question of to what extent classes of “natural” supersymmetric models are within the reach of HE-LHC and can be discovered or excluded conclusively. Examples of specific model scenarios were studied during the Workshop, as summarized in Fig. 2. Colored points correspond to parameter configurations of several supersymmetric models inspired by the requirement of a natural solution to the hierarchy problem. While HL-LHC can only cover part of the parameter space of the illustrated models, HE-LHC covers it entirely. The HE-LHC would allow for a  $5\sigma$  discovery of most models via the observation of both gluinos and stops. For the models labeled by red (green) dots, the  $5\sigma$  discovery is limited to the stop (gluino).

If the coloured states are close in mass to the lightest supersymmetric particle (LSP), the amount of missing transverse momentum ( $E_T^{\text{miss}}$ ) in the event is decreased. The typical multijet +  $E_T^{\text{miss}}$  SUSY searches are less sensitive and must be replaced with monojet-like analyses. Prospect studies show that if for example the gluino-LSP mass splitting is assumed to be 10 GeV, gluino masses can be excluded up to 2.6 TeV. If the lightest coloured state is the stop, and the  $\tilde{t}$ -LSP splitting is such that final states include very off-shell  $W$  and  $b$ -jets,  $\tilde{t}$  masses up to about 1 TeV could be excluded, extending the HL-LHC reach by about a factor of two.

The electroweakino sector of supersymmetry presents a particular challenge for hadronic machines. If the LSP is pure higgsino or wino, there is a very small neutralino-chargino mass splitting ( $\sim 340$  MeV,  $\sim 160$  MeV respectively) and the chargino has a correspondingly long lifetime ( $c\tau \sim 5, 1$  cm respectively). The value of  $E_T^{\text{miss}}$  is again small unless the pair produced electroweakinos recoil against an ISR jet. Taking into account contributions from both chargino and neutralino production, the monojet search will deliver a sensitivity for exclusion (discovery) of winos up to  $\sim 600$  GeV (300 GeV) and of higgsinos up to  $\sim 400$  GeV (150 GeV). Taking advantage of the long lifetime of the charginos, searches for disappearing charged tracks can be performed. Considering a detector similar to the ones available for HL-LHC, winos below  $\sim 1800$  GeV (1500 GeV) can be excluded (discovered), while the equivalent masses for Higgsinos are  $\sim 500$  (450) GeV (see Fig. 3). While these results come short of covering the full range of masses for electroweakinos to be a thermal relic and account for all of DM, the mass range accessible to HE-LHC greatly extends the HL-LHC potential and can be complementary to the indirect detection probes using gamma rays from dwarf-spheroidal galaxies.

## 2.2 Dark Matter

Monojet searches, as well as monophoton and vector-boson-fusion production searches, might be sensitive to generic weakly interactive dark matter candidates beyond compressed SUSY scenarios. Analyses of the reach of the HE-LHC under various assumptions of the structure of the DM-SM coupling have been carried out. Models characterized by the presence of an extended Higgs sector, with Higgs doublets mixing with an additional scalar or pseudo-scalar mediator that couples to DM have been studied assuming associate production of DM with a pair of top quarks. Using leptonic decays of the tops, a fit to the distribution of the opening angle between the two leptons can help distinguish signal from SM processes, after other background-suppressing selections. Assuming the DM is lighter than half the mediator mass, a scalar or pseudoscalar mediator can be ruled out at 95% CL up to 900 GeV using this technique, a factor of two higher in mass compared to the HL-LHC bounds.

If a dark sector exists and contains heavy coloured particles,  $\mathcal{Q}$ , nearly degenerate with the DM and decaying to DM and SM coloured particles, a monojet topology could be again the most sensitive. The rate and shape of the monojet distribution depend upon the mass, spin and colour representation of  $\mathcal{Q}$ . Fermionic colour triplet  $\mathcal{Q}$  could be discovered up to 1.1 TeV at the HE-LHC, a fermionic octet will be ruled out if lighter than 1.8 TeV, and a scalar colour triplet almost degenerate in mass to the DM could be probed up to masses of 600 GeV. Should an excess be observed, the identification of the spin and colour representation will require NNLO precision for the predictions of the SM backgrounds. Analyses of double-ratios of cross sections at varying  $p_T$  could be utilized to partially cancel uncertainties.

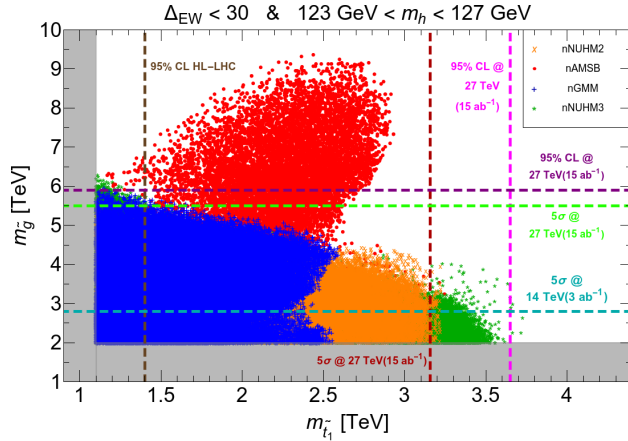


**Figure 2.** Discovery reach at the HE-LHC for gluinos and stops in various supersymmetric models, compared to the HL-LHC reach and to the expectations of classes of natural supersymmetric models. The relevant areas lie under the horizontal lines (for the gluino) and to the left of the vertical lines (for the stop). From Ref. [4].

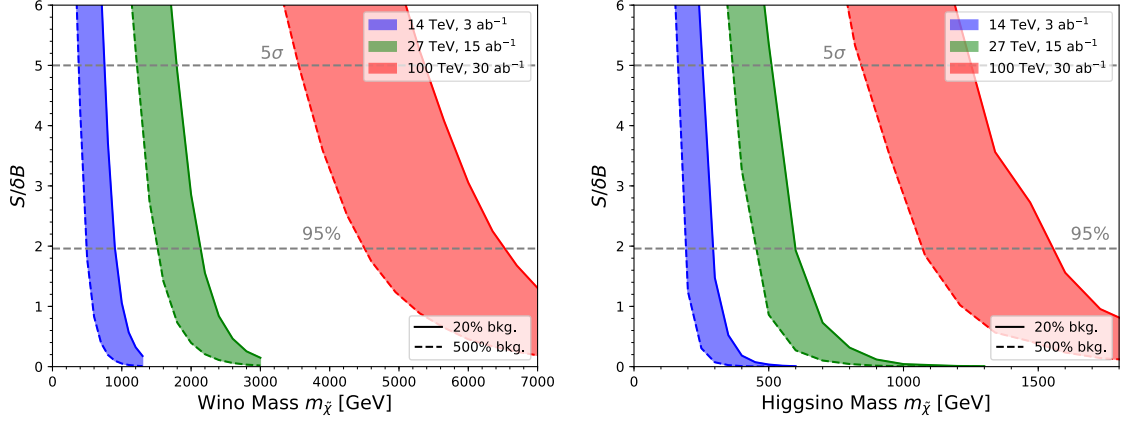


**Figure 3.** The reach of HE-LHC in the search for a wino (left) or higgsino (right) DM WIMP candidate, using a disappearing charged track signature. The solid and dashed lines correspond to modifying the central value of the background estimate by a factor of five. The results are compared to the reach of HL-LHC, and FCC-hh. From Ref. [4].

### 2.3 Resonance searches

Searches for heavy resonances will greatly benefit from the increased partonic energy of HE-LHC. If the resonance is narrow, data-driven searches can be carried out, while, if it is wide, it will require a precise understanding of the SM backgrounds. The HE-LHC can expect to approximately double the HL-LHC mass reach for dijet resonances. For instance, the reach for an excited quark  $Q^*$  decaying to dijets will be up to 14 TeV, with discovery potential up to 12 TeV. Dilepton resonances, e.g.  $Z'$ , are present in many gauge extensions of the SM. The exact reach in any model depends upon the coupling to light quarks and the branching fraction to charged leptons. A  $Z'$  whose couplings to SM quarks and leptons are as in the SM, a so-called sequential  $Z'_{SSM}$ , can be used as reference to evaluate the discoverability at the HE-LHC. In the dilepton ( $ee, \mu\mu$ ) channel,  $Z'_{SSM}$  up to  $\sim 13$  TeV could be discovered. In the di-tau channel, where hadronic  $\tau$  reconstruction is more challenging, the discovery reach is about  $\sim 6$  TeV. In the di-top channel, a  $Z'_{SSM}$  decaying into a top-quark pair could be discovered up to 6 TeV and excluded up to 8 TeV. The same search interpreted in terms of Randall–Sundrum Kaluza–Klein gluons lead to sensitivity up to 10.7 TeV, which constitutes a 4 TeV extension with respect to HL-LHC, with discovery reach up to 10 TeV as shown in Fig. 4 (left). A collection of exclusion and discovery reaches for these and other models is given in Table 1. The prospects to determine the nature of a  $Z'$  discovery are discussed in Sect. 3.

**Table 1.** 95%CL limits and  $5\sigma$  discovery reach for various resonances [4]: excited quarks  $Q^*$ , Randall-Sundrum gluons  $g_{RS}$  and gravitons  $G_{RS}$ ,  $Z'$  bosons in the sequential SM and in top-colour (TC) models.

Process	95%CL	$5\sigma$	Process	95%CL	$5\sigma$
$Z'_{SSM} \rightarrow e^+e^-/\mu^+\mu^-$	13 TeV	13 TeV	$G_{RS} \rightarrow WW$	8 TeV	7 TeV
$Z'_{SSM} \rightarrow \tau^+\tau^-$	6 TeV	6 TeV	$g_{RS} \rightarrow t\bar{t}$	10.7 TeV	9.4 TeV
$Z'_{TC} \rightarrow t\bar{t}$	10 TeV	8 TeV	$Q^* \rightarrow jj$	14 TeV	12 TeV

Gauge extensions of the SM also often contain new heavy charged vector bosons,  $W'$ . One promising search channel for these new particles is the  $WZ$  final state. More generally BSM models can contain resonances decaying to di-bosons  $WZ/WW$ . Searching for a RS graviton  $G_{RS}$  resonance in  $WW$  final states exploiting the all-hadronic signature presents a considerable challenge and requires dedicated identification of boosted  $W$ -jets. The estimated reach is  $\sim 8$  TeV, almost a factor of two increase with respect to the HL-LHC. Diboson searches in  $WW \rightarrow \ell\nu qq$  final states are sensitive also to heavy vector triplet (HVT) model produced via  $ggF/q\bar{q}$ . HVT  $Z'$  masses up to 11 TeV can be excluded by HE-LHC (see Fig. 4 - right), extending the HL-LHC reach by about 6 TeV.

Searches for top partners decaying to a top and a  $W$  boson in the same-sign dilepton signature can lead to discovery up to more than 2 TeV, with the possibility to discriminate left- and right-handed couplings at the  $2\sigma$  level in the full accessible discovery range.

Models related to the generation of the observed pattern of neutrino masses and mixings offer a variety of signatures that could profit from the high energy available at HE-LHC. For instance, searches for lepton flavour violating (LFV) final states with two opposite-sign different-flavour leptons and two jets arising from the production of a heavy pseudo-Dirac neutrino and a SM lepton could test heavy neutrino masses, in seesaw models, up to more than 1 TeV. In left-right symmetric models, a

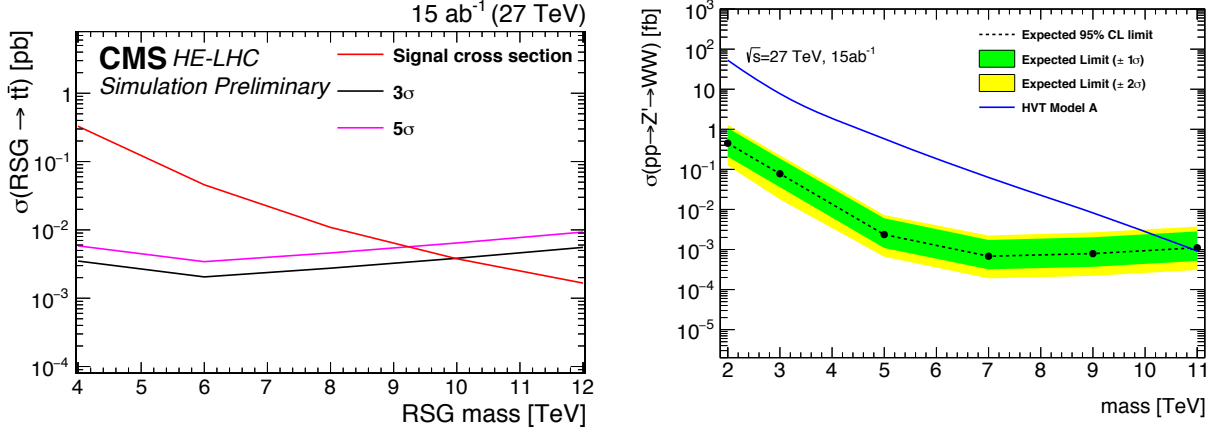


**Figure 4.** Left: Discovery reach for a RS Graviton decaying to  $t\bar{t}$  at the HE-LHC. Right: Upper limit for a HVT  $Z' \rightarrow WW$  via  $ggF/q\bar{q}$  production. From Ref. [4].

right-handed heavy  $W_R$  boson decaying to a Majorana neutrino can be discovered up to  $\sim 10.5$  TeV with  $5 \text{ ab}^{-1}$ , and excluded up to masses of around  $\sim 16$  TeV with an integrated luminosity of  $15 \text{ ab}^{-1}$ . This increases the reach of HL-LHC by about 10 TeV. Doubly charged scalars in type-II seesaw models, can also be searched for in multi-lepton signatures, with a reach in the 1.5 TeV region. Heavy leptons in type-III seesaw models, giving rise to final states with two leptons, jets and  $b$ -jets can be excluded (discovered) up to 3.8 (3.2) TeV. For comparison, the exclusion reach for the HL-LHC is about 1.6 TeV.

#### 2.4 Exploring the largest $Q^2$ values

The increase in energy and integrated luminosity at the HE-LHC will allow to probe QCD at the highest values of  $Q^2$ , searching for deviations induced by new physics at energy scales well beyond the reach of the HL-LHC. The HE-LHC kinematic reach will extend up to 10 TeV in the jet transverse momentum  $p_T$  and up to 22 TeV in the di-jet invariant mass  $m_{jj}$ . The inclusive production of isolated-photons and jets will reach up to 5 TeV in the photon  $E_T$  and jet  $p_T$ , and up to 12 TeV in the photon-jet invariant mass. In Table 2, event yields for various processes involving top quarks are listed. The typical increase in inclusive event yield for top quark production will be roughly a factor 20, providing ample statistics for all single-top processes as well as for the associated production of top quarks with heavy particles. The expected increase for  $t\bar{t}$  events with  $p_T^{\text{top}} > 2$  TeV is about a factor 500. Production of events with four top quarks in the final state is enhanced by about a factor of 40, leading to an expected statistical uncertainty in the cross section measurement of 1%.

**Table 2.** Approximate event yields at HL-LHC ( $3 \text{ ab}^{-1}$ ) and HE-LHC ( $15 \text{ ab}^{-1}$ ) for top quark production, for inclusive and high- $Q^2$   $t\bar{t}$  final states, for single top production in the  $t$ -channel,  $s$ -channel, associated  $Wt$  production, for  $t$ -channel production in association with a  $Z$  boson, and for  $t\bar{t}W$ ,  $t\bar{t}Z$ ,  $t\bar{t}H$ ,  $tH$  and  $t\bar{t}\bar{t}$  inclusive final states. The values for single top quark processes refer to the sum of top quark and top antiquark production. From Ref. [2].

Process	HL-LHC	HE-LHC
$t\bar{t}$	$3 \times 10^9$	$5 \times 10^{10}$
$t\bar{t}$ ( $p_T^{\text{top}} > 2 \text{ TeV}$ )	$3 \times 10^2$	$1.5 \times 10^5$
$t$ -channel	$8 \times 10^8$	$1 \times 10^{10}$
$Wt$	$2 \times 10^8$	$2 \times 10^9$
$s$ -channel	$3 \times 10^7$	$4 \times 10^8$
$tqZ$	$3 \times 10^6$	$6 \times 10^7$
$t\bar{t}W$	$2 \times 10^6$	$4 \times 10^7$
$t\bar{t}Z$	$3 \times 10^6$	$7 \times 10^7$
$t\bar{t}H$	$2 \times 10^6$	$4 \times 10^7$
$tH$	$3 \times 10^5$	$6 \times 10^6$
$t\bar{t}\bar{t}$	$5 \times 10^4$	$2 \times 10^6$

### 3 Exploring the properties of possible LHC discoveries

In this section the potential of HE-LHC to further scrutinise possible future discoveries at the LHC is outlined. Should future runs of the LHC find evidence of new phenomena, the HE-LHC would increase the statistics of these signals and make it possible to analyse their properties in more detail, or to provide conclusive evidence of unconfirmed deviations from the SM. Many interesting scenarios of new physics, e.g. supersymmetry, present a spectrum of multiple states distributed over a broad mass range and the doubling of LHC's energy would be a useful additional feature to complement an LHC discovery.

Figure 5 shows the increase expected in event yield at the HE-LHC, relative to HL-LHC, for final states of mass  $M$  produced through various partonic initial states ( $gg$ ,  $qg$  and  $q\bar{q}$ ), as a function of  $M$ . This growth in the rate takes into account an increase by a factor of 5 in integrated luminosity ( $15$  vs  $3 \text{ ab}^{-1}$ ), in addition to the partonic luminosity increase. It is clear that the higher energy of HE-LHC is particularly beneficial in the case of the heaviest objects, where the gain can reach several orders of magnitude whereas, for the study of low mass systems, the luminosity is the key factor. In this latter case, a careful study of the overall experimental conditions (backgrounds and pile-up) is necessary for a more reliable estimate of the actual gain obtained with the HE-LHC.

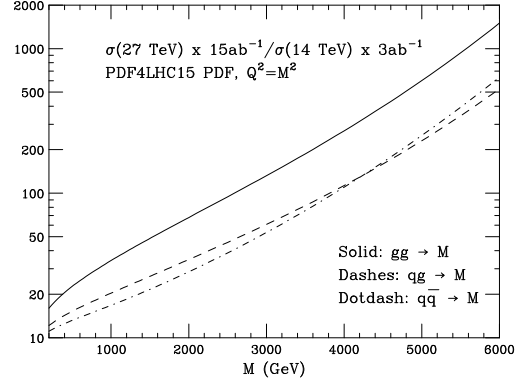


**Figure 5.** Statistics increase at HE-LHC, relative to HL-LHC, for the production of a system of mass  $M$ , in the three production channels  $gg$ ,  $qg$  and  $q\bar{q}$ .

#### 3.1 Characterization of a $Z'$ gauge boson

As a specific example, we study the case of a new  $Z'$  gauge boson, hypothetically observed at the HL-LHC in the dilepton channel. Considering today's statistics and limits, future LHC data may be sufficient to support an evidence or discovery, but not for a complete determination of the properties of the new particle. The model discrimination requires, for example, a higher-statistics study of angular and rapidity distributions. This can be done at HE-LHC, using for example  $A_{FB}$ ,  $r_y$  and  $\sigma \times \text{BR}$ . Here  $r_y = N(Z', |y| < 0.5) / N(Z', 0.5 < |y| < 2.5)$ , while  $A_{FB}$  is defined as the asymmetry between the number of events in which the lepton moves forward or backward (in the  $Z'$  rest frame) relative to the  $Z'$  longitudinal direction. The left plot in Fig. 6 shows the correlation between  $A_{FB}$  and  $r_y$  for the  $Z'$  of different models, with a common mass of 6 TeV, towards the edge of observability at HL-LHC. The interference between the signal and the SM DY amplitude is included, and events within a mass window of 200 GeV around the resonance peak are used. The studies assume systematics of 2% for the measurement of  $r_y$  and  $A_{FB}$ , and 5% for  $\sigma \times \text{BR}$ . These systematics dominate the uncertainties reported in the figures and are likely to be reduced significantly after more dedicated analyses. A further handle to discriminate among different models is the study of hadronic decays to light,  $b$  and  $t$  quarks. The expected precision of the measurements is shown in the right side of Fig. 6. With the exception of the  $\eta$  and  $\psi$  models, the predictions of which are very similar for all considered observables, all other models can be separated through a combination of different observations. For example, the SSM and  $\psi$  models, which have very close predictions for  $r_y$  and  $A_{FB}$ , have measurably different fractions of  $b$  or  $t$  final states.

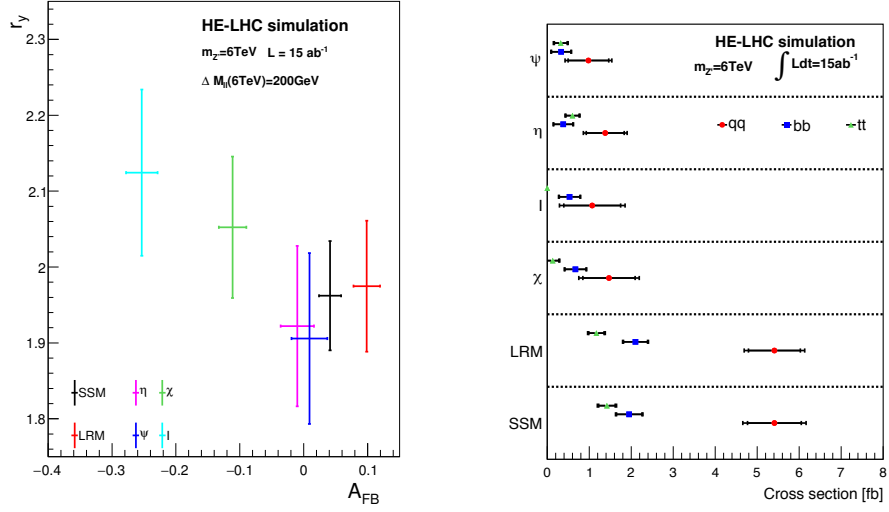
#### 3.2 Flavour anomalies

A set of anomalies reported in  $B$  decays point to the violation of lepton flavour universality. If confirmed, these anomalies would revolutionize particle physics, and open the search for their microscopic origin. Current interpretations suggest the presence of heavy resonances, either a  $Z'$  or a leptoquark, coupling to muons and  $b$ -quarks. The HE-LHC will be able to cover an ample region of the parameter space allowed by flavor constraints, with an exclusion (discovery) reach up to 10 (7) TeV for the  $Z'$  boson, depending on the assumptions on the  $Z'$  couplings structure and strength. Figure 7 shows the coupling/mass domains that the HE-LHC would be sensitive to, at 95%CL. The left plot considers a minimal case, in which the only  $Z'$  coupling to quarks involves the  $b\bar{s}$  pair. The reach is limited by the low production rate for  $b\bar{s}(s\bar{b}) \rightarrow Z'$ . The right plot corresponds to models where the  $Z'$  couples to quarks via the current  $\sum_{q,q'} V_{iq} V_{iq'} \bar{q} \gamma_\mu q'_L$  ( $q, q' = d, s, b$ ). In this case, the production channel  $d\bar{s}(s\bar{d}) \rightarrow Z'$  amplifies the signal, giving full coverage of the allowed parameter space. Pair produced leptoquarks, on the other hand, can be excluded up to masses of 4.2 TeV, depending on coupling's strength. These masses are typically a factor of 2 to 2.5 higher than the HL-LHC sensitivity.

### 4 Measurements of Higgs properties, and studies of EW symmetry breaking

With the increase in centre-of-mass energy and luminosity, the Higgs physics programme at HE-LHC will considerably extend the precision reach of the entire HL-LHC program. Measurements of the Higgs boson trilinear self-coupling, of elusive decay

**Figure 6.** Left: correlation between the observables  $r_\gamma$  and  $A_{FB}$ , described in the text, for various  $Z'$  models. Right: fitted cross-section of the three hadronic analyses. Statistical and full uncertainties are shown on each point. From Ref. [4].



modes (e.g.  $H \rightarrow c\bar{c}$ ), of rare (e.g.  $H \rightarrow Z\gamma$ ), invisible or forbidden decays become accessible. At the same time, Higgs boson production can be explored at very large transverse momenta. Projections presented in this section are exploratory and provide qualitative results, due to the absence of clearly defined reference detectors, and in view of the highly challenging pile-up environment. Several approaches have been followed to address this issue, typically assuming experimental performances similar to those currently achieved by LHC detectors. Other studies focused on Higgs bosons produced at finite transverse momentum ( $p_T > 50$  GeV), to reduce the impact of pile-up. The selection of fiducial regions in  $p_T$  and rapidity, furthermore, allows measurements of the ratios of rates for different final states, free of uncertainties related to the production dynamics and to luminosity.

**Table 3.** Higgs production event rates for selected processes at 27 TeV ( $N_{27}$ ) and statistical increase with respect to the statistics of the HL-LHC ( $N_{27} = \sigma_{27 \text{ TeV}} \times 15 \text{ ab}^{-1}$ ,  $N_{14} = \sigma_{14 \text{ TeV}} \times 3 \text{ ab}^{-1}$ ).

	$gg \rightarrow H$	VBF	WH	ZH	$t\bar{t}H$	HH
$N_{27}$	$2.2 \times 10^9$	$1.8 \times 10^8$	$5.4 \times 10^7$	$3.7 \times 10^7$	$4 \times 10^7$	$2.1 \times 10^6$
$N_{27}/N_{14}$	13	14	12	13	23	19

The statistics expected for some reference production processes, and the increase with respect to the HL-LHC, are shown in Table 3. The Higgs samples will typically increase by a factor between 10 and 25, in part as a result of the 5 times larger luminosity, leading to a potential reduction in the statistical uncertainties by factors of 3 to 5. The biggest improvements arise for the channels favoured by the higher energy, such as  $t\bar{t}H$  and HH.

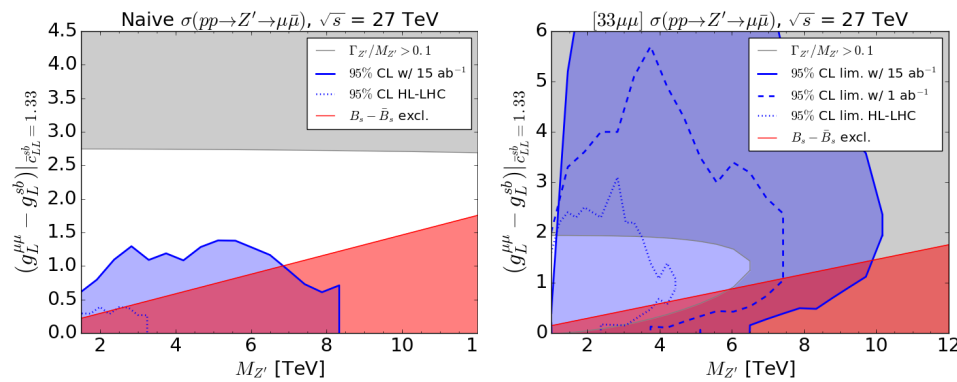


**Figure 7.** Projected 95%CL sensitivities at HE-LHC (blue regions) for  $Z'$  models explaining the  $R_{K^{(*)}}$  anomaly, assuming narrow-width resonances ( $\Gamma < 0.1M_{Z'}$ ). The red region is excluded from  $B_s - \bar{B}_s$  mixing measurements. See Refs. [4, 5] for the details.

The potential for the measurement of the Higgs boson trilinear coupling at the HE-LHC has been estimated with methods and in channels similar to those used at the HL-LHC. Extrapolation studies from the current experiments and from phenomenological studies have been carried out in the two most sensitive  $HH$  channels at the HL-LHC ( $b\bar{b}\gamma\gamma$  and  $b\bar{b}\tau^+\tau^-$ ). Several studies were made under different experimental performance and systematic uncertainty assumptions (in some cases neglecting systematic uncertainties), yielding results covering the wide range of precision estimates presented here. At the HE-LHC the  $HH$  signal would be observed unambiguously and the combined sensitivity on the trilinear coupling  $\kappa_\lambda$ , assuming the SM, is expected to reach a precision of 10% to 20% from the combination of these two channels alone. A comparison of the HE-LHC sensitivity to that of the HL-LHC is displayed in Fig. 8, showing that the secondary minimum still visible in the HL-LHC study is unambiguously excluded at HE-LHC.

These studies do not include the additional decay channels that have already been studied for HL-LHC, and of others that could become relevant at the HE-LHC. Exclusive production modes are also very interesting to take into consideration for this measurement. The potential improvements from these have not been assessed yet.

The measurement of the couplings of the Higgs boson at HL-LHC relies either on the assumption that no additional undetected contribution to the Higgs boson width is present, or that the couplings of the Higgs boson to vector bosons do not exceed those expected in the SM. In both cases, the foreseen precision in the measurements of most Higgs boson couplings at the HL-LHC is currently limited by the theoretical uncertainty on the signal predictions. The significantly larger dataset and the increase in centre-of-mass energy at HE-LHC would reduce the statistical uncertainty of these measurements to being negligible. To match the overall precision of the experimental measurements, the extraction of the couplings of the Higgs boson to photons, gluons, W, Z, taus, and b quarks will require significant theoretical improvements in the precision of the theoretical predictions for the signals.

For rare decay processes such as the dimuon channel, from an extrapolation of the HL-LHC projections, a precision of approximately 2% on the coupling modifier should be achievable. With the current theoretical systematic uncertainties on the signal and the backgrounds, the direct measurement of the Higgs coupling modifier to top quarks is expected to reach a precision of approximately 3%. While the substantial additional amount of data at various centre-of-mass energies will undoubtedly be useful to further constrain the systematic modelling uncertainties and further progress in theoretical predictions will be achieved, the potential improvements have not been quantified. Assuming an improvement of the theoretical uncertainties of a factor of 2, the precision on the  $t\bar{t}H$  coupling would reach approximately 2% (the experimental systematic uncertainty alone is approximately 1%, assuming performances similar to current LHC experiments). The significant gain in precision will be obtained mostly through ratios of couplings. Studies have shown that the ratio of the  $t\bar{t}H$  to  $t\bar{t}Z$  ratio could be measured at close to the percent level.

In the range of Higgs boson transverse momenta between 50 and 500 GeV, a precision in the range of 2-4% is achievable for the ratios  $\text{BR}(H \rightarrow \mu\mu)/\text{BR}(H \rightarrow \gamma\gamma)$  and  $\text{BR}(H \rightarrow 4\ell)/\text{BR}(H \rightarrow \gamma\gamma)$ , and therefore of order 1-2% for the ratios of the relevant Higgs couplings (see Fig. 9). At HE-LHC energies  $H \rightarrow c\bar{c}$  production increases relative to backgrounds, and may be observable with inclusive searches by ATLAS, CMS, and LHCb, dependent on  $c$ -tagging systematic uncertainties. Unfortunately, at the HE-LHC, exclusive searches, kinematic limits, and global fits are not expected to reach the SM level for the  $u$ ,  $d$ ,  $s$ , and  $c$  Yukawas.

Precision measurements provide an important tool to search for BSM physics associated to mass scales beyond the LHC direct reach. The EFT framework, where the SM Lagrangian is supplemented with higher dimension operators  $\sum_i c_i^{(6)} \mathcal{O}_i^{(6)}/\Lambda^2 + c_i^{(8)} \mathcal{O}_i^{(8)}/\Lambda^4 + \dots$ , allows one to systematically parametrise BSM effects and how they modify SM processes. These operators can either modify SM amplitudes, or generate new amplitudes. In the former case, the best LHC probes are, for example, precision measurements of Higgs branching ratios. In the case of the operator  $\mathcal{O}_H$ , for example, the constraints in Fig. 10 translate into a sensitivity to the Higgs compositeness scale  $f > 2$  TeV, corresponding to a new physics mass scale of 25 TeV for an underlying strongly coupled theory.

Effects associated with new amplitudes grow quadratically (for dimension-6 operators) with the energy. The higher centre-of-mass energy and larger dataset of HE-LHC make it possible to greatly extend the measurable range in the Higgs

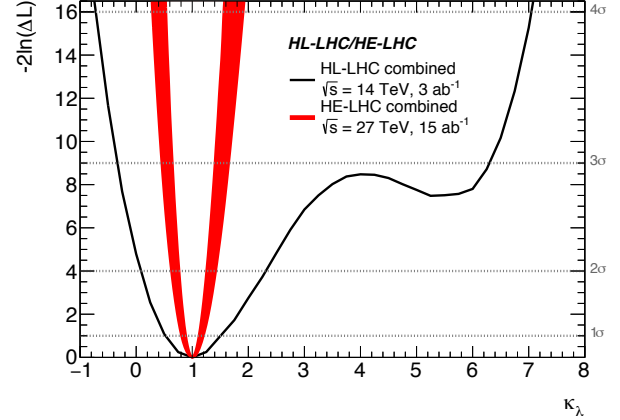


**Figure 8.** Expected sensitivity for the measurement of the of the Higgs trilinear coupling through the measurement of direct  $HH$  production at HE-LHC. From Ref. [3].

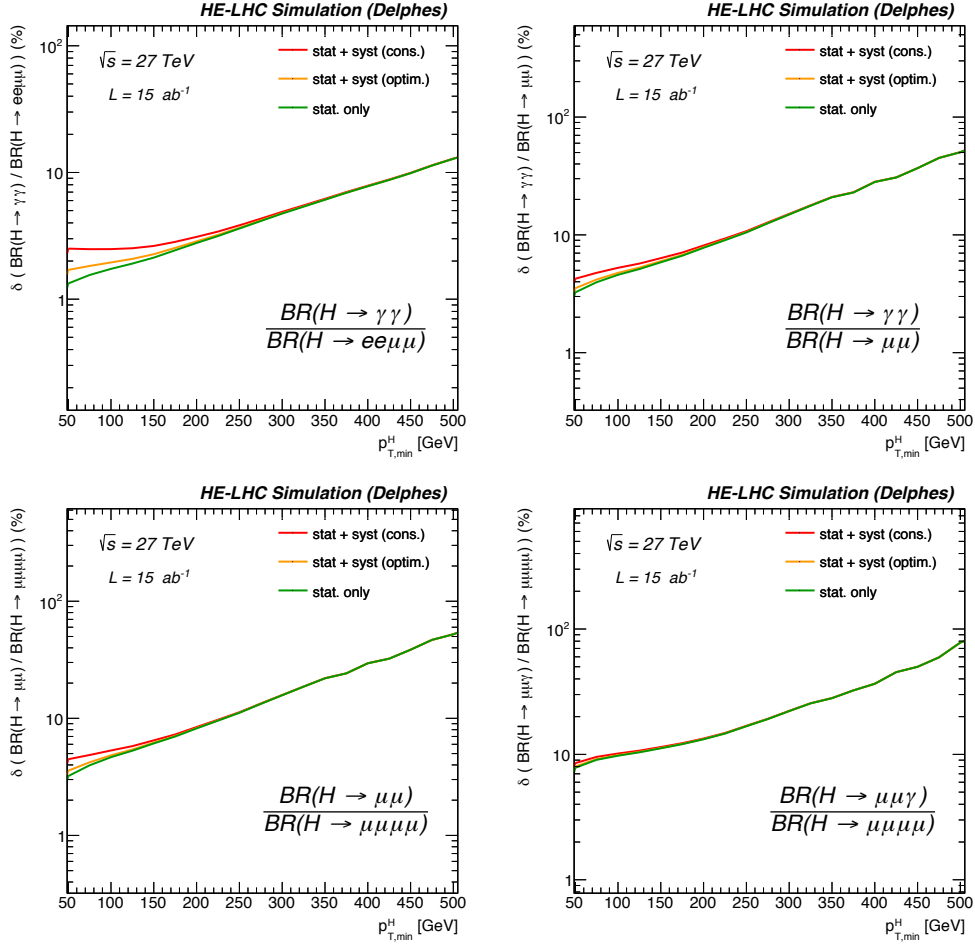


**Figure 9.** Projected precision for the measurement of ratios of rates of different Higgs final states, in the  $gg \rightarrow H$  production channel. The label "lumi" indicates the inclusion of a 1% overall uncertainty. The systematics labeled "syst" reflects today's uncertainties on detection efficiencies. The systematics of conservative scenario (cons) is twice as large as the reference one (optim).

transverse momenta, providing a new opportunity: a 10% measurement at 1 TeV energy corresponds roughly to a permille precision measurement at the Higgs mass. In the context of EW physics this will allow to test, via Drell-Yan processes and the operators  $\mathcal{O}_{2W,2B}$ , energy scales of order 25 TeV; or, via  $WZ$  diboson processes, mass scales of roughly 6 (100) TeV if the underlying new physics is weakly (strongly) coupled. Figure 10 shows the results of a global fit to observables in Higgs physics, as well as diboson and Drell-Yan processes at high energy.

Another important high-energy measurement concerns the scattering of longitudinally polarised vector bosons: departures from its SM value could betray a composite nature of the Higgs. The decomposition of measurements of VBS cross-sections into the polarised components based on the decays of the individual vector bosons is experimentally challenging. Preliminary studies show that, thanks to pile-up mitigation techniques that retain Run-2 performance of hadronically decaying  $W/Z$ -boson tagging, the precision on the VBS cross section measurement in the semileptonic  $WV + jj \rightarrow \ell\nu + jjjj$  channel can be reduced from 6.5 % (HL-LHC) to about 2 % at HE-LHC. From this measurement and from the measurement of the EW production of a  $Z$  boson pair, the purely longitudinal final state of the  $WW$  and  $ZZ$  scattering processes can be extracted with a significance of  $5\sigma$  or more. Similarly, the reach for vector-boson-scattering will be extended by roughly a factor of two in the energy scale of BSM physics, i.e. the sensitivity of the HE-LHC to Wilson coefficients,  $f/\Lambda^4$ , of dimension eight operators, which describe anomalous quartic gauge couplings, improves by a factor 10-20.

BSM theories generally predict the Higgs couplings to deviate from the SM predictions. In parallel, the HE-LHC will have a broad reach for models predicting exotic decays of the 125 GeV Higgs boson (e.g. decays including intermediate BSM

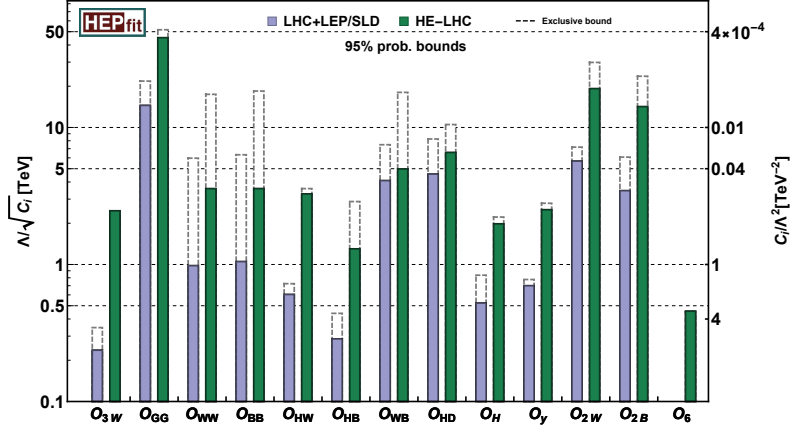


**Figure 10.** Summary of constraints on the EFT operators considered. The shaded bounds arise from a global fit of all operators, those assuming the existence of a single operator are labeled as "exclusive". From Ref. [3].

particles that are long lived, decays including light scalars, light dark photons or axion-like particles).

The large variety of BSM Higgs signals studied at HL-LHC can be probed and discovered at the HE-LHC. Due to the very large production rate of the 125 GeV Higgs boson, the HE-LHC can have an unprecedented reach for Higgs exotic rare decays. For example are the  $h \rightarrow Z_D Z_D \rightarrow b\bar{b}\mu\mu$  and  $h \rightarrow Z_D Z_D \rightarrow 4\ell$  decays (where  $Z_D$  is an axion-like particle or dark photon), for which branching ratios as small as  $10^{-5}$  and  $10^{-8}$  could be probed, respectively.

The collider reach for additional heavy Higgs bosons will also extend to higher masses. For example, the reach for  $pp \rightarrow S \rightarrow hh$ , with  $h$  the 125 GeV Higgs boson and  $S$  a new Higgs boson, can extend to  $S$  masses that are 1.5-2 times heavier than the masses probed by the HL-LHC.

## 5 Flavour

The LHC has proven to be an excellent facility for the study of quark flavour. However, even after completion of the HL-LHC, the precision of a rich set of observables sensitive to new physics would still be statistics limited. A factor of 10 increase in integrated luminosity, delivering  $3 \text{ ab}^{-1}$  to an upgraded LHCb detector, and the doubling of the  $b$  quark production cross section, would give the HE-LHC a compelling opportunity to further enhance this sensitivity and fully exploit its flavour physics potential. A few highlights of this reach are listed here. Using rare hadronic  $B$  decays, the CKM phase  $\gamma$  is determined today to  $\sim 5^\circ$ . At the HE-LHC  $\gamma$  would be determined to  $< 0.1^\circ$  with several different decay modes, while  $\beta$  could be extracted from several tree-level decays. By suppressing the theoretical systematics, these measurements would subject the CKM unitarity to uniquely stringent tests. The theoretically clean ratio  $\text{BR}(B_d \rightarrow \mu^+\mu^-)/\text{BR}(B_s \rightarrow \mu^+\mu^-)$  would be measured with  $\mathcal{O}(\%)$  precision, a powerful probe of new physics, with reach well above 10's of TeV. There would be further exciting opportunities with CP violation and mixing with charm hadrons, rare kaon decays, and unexpected discoveries with exotic hadrons. The HE-LHC would also strengthen the role of high- $p_T$  measurements in flavour physics, as shown for example in Section 3.2. The large data sets of top quarks, shown in Table 2, will furthermore improve by one order of magnitude the sensitivity to top-quark FCNC decays, relative to the HL-LHC.

## 6 QCD matter at high density and temperature

HE-LHC would allow Pb-Pb collisions at  $\sqrt{s_{NN}} = 10.6 \text{ TeV}$  and p-Pb collisions at  $\sqrt{s_{NN}} = 17 \text{ TeV}$ . On the basis of first extrapolations of LHC and FCC-hh performance, the increase in integrated luminosity per run with respect to the LHC is expected to be of a factor about two, i.e.  $L_{\text{int}} \sim 6 \text{ nb}^{-1}$  in a typical one-month run. Detailed studies will be carried out in the future. A larger increase in terms of nucleon-nucleon (NN) luminosity could be achieved with collisions of nuclei lighter than Pb. For example Xe-Xe (11.5 TeV) would give an increase of  $L_{\text{int,NN}}$  larger by a factor 2-3 than Pb-Pb, while still producing a Quark-Gluon Plasma (QGP) with a volume and energy density similar to those of Pb-Pb at LHC energies [6]. Qualitatively-novel scientific motivations for a heavy-ion programme at the HE-LHC are summarised here.

### 6.1 Novel probes of quark-gluon thermalization and of the QGP equation-of-state

Increasing the centre-of-mass energy in heavy-ion collisions leads to the creation of initially denser and hotter strongly-interacting systems that expand for a longer duration and over a larger volume, thereby developing stronger collective signals. Extrapolations of Pb–Pb measurements indicate that the initial energy density increases by a factor about 1.4 from LHC to HE-LHC. The HE-LHC collision energies reach closer to the range of temperatures ( $T \sim 1$  GeV) where charm quarks start to contribute as active thermal degrees of freedom in the QGP equation of state in addition to u, d, s, quarks, thus playing a novel role in QCD equilibration processes. The left panel of Fig. 11 shows a prediction of secondary (thermal) charm production from  $gg$ ,  $q\bar{q}$ ,  $qg$  processes in the QGP, for central Pb–Pb collisions at HE-LHC energy. The secondary production is shown as an increase with time of the total  $c\bar{c}$  yield per unit of rapidity. The increase with respect to the initial production in hard-scattering processes could reach up to 20% and it is sensitive to the thermalisation time of the QGP as well as to its temperature profile in time.

### 6.2 Characterisation of dense QCD matter through hard-scattering processes

High-energy partons produced in heavy-ion collisions are known to undergo QCD energy loss and strong medium-induced modifications, often referred to as jet quenching. Jet quenching measurements provide quantitative information on the transport properties of hot and dense QCD matter. The HE-LHC would provide much larger abundance of hard-scattering processes than the LHC, as well as novel probes such as boosted top quarks and, potentially, the Higgs boson (see central panel of Fig. 11). For example, the production cross sections for jets with  $p_T > 100$  GeV/c (as well as for the Higgs boson) and for top quarks increase by factors of four and six, respectively. A remarkable physics case is provided by high-momentum (thus, highly boosted)  $t \rightarrow W \rightarrow q\bar{q}$  decay chains, which are promising probes of the time evolution of the QGP opacity to hard partons and, thus, of its density: the right panel of the Fig. 11 shows that, while at LHC the study can be limited to probing times of about 1 fm/c, HE-LHC would give access to a range up to  $\sim 5$  fm/c, to be compared with a lifetime of the QGP phase of about 10 fm/c. This gain results from the larger and harder  $p_T$ -differential cross section of top quarks.

### 6.3 Exploration of parton densities in a ultra-dense kinematic domain at low $x$

The higher centre-of-mass energy of HE-LHC gives access, in the initial state of heavy-ion collisions, to a wide previously-uncharted kinematic range at low  $x$  and  $Q^2$ , where parton densities become very large and may reach the non-linear QCD regime known as “parton saturation”. The onset of this regime is usually discussed in terms of the saturation momentum  $Q_S^2$ , defined as the scale at which the transverse area of the nucleus is completely saturated and gluons start to overlap. It can be shown that for nuclei  $Q_S^2 \sim A^{1/3} (\sqrt{s_{NN}})^\lambda e^{\lambda y}$ , with the mass number  $A$  and  $\lambda \approx 0.3$  [6]. Therefore, the kinematic region of high gluon density is best accessed at a high- $\sqrt{s_{NN}}$  hadron collider with measurements at moderate  $p_T \approx 2\text{--}4$  GeV/c and forward rapidity, which probe small  $x$  and perturbative  $Q^2$  values around  $Q_S^2$ . These studies allow establishing the existence of the saturation regime of QCD and validating the different approaches to describe non-linear parton evolution. The HE-LHC extends the small- $x$  coverage by a factor of two with respect to the LHC, down to  $x \approx 5 \times 10^{-6}$  at a rapidity of  $y \approx 5$  in p–Pb collisions.

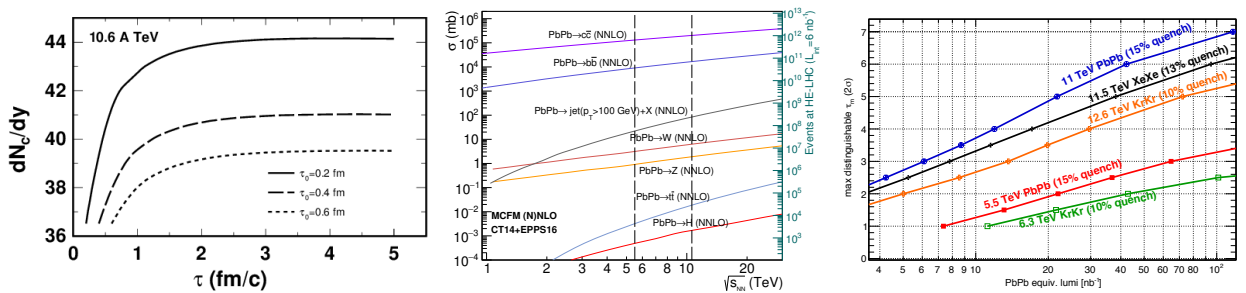


**Figure 11.** Left: yield of secondary charm production in central Pb–Pb collisions as a function of time. Middle: NNLO cross sections for various hard-scattering processes as a function of  $\sqrt{s_{NN}}$  in Pb–Pb collisions (the right axis indicates the expected number of events per Pb–Pb run at HE-LHC). Right: maximum time in the QGP evolution that can be probed with boosted top topologies as a function of Pb–Pb-equivalent integrated luminosity in various colliding systems at LHC and HE-LHC. Figures from Ref. [6].